Physics of Plasmas ARTICLE pubs.aip.org/aip/pop

DC electric field generation and distribution in magnetized plasmas

Cite as: Phys. Plasmas **30**, 072509 (2023); doi: 10.1063/5.0142813
Submitted: 17 January 2023 · Accepted: 24 June 2023 ·
Published Online: 13 July 2023

Jean-Marcel Rax,[1,2] Renaud Gueroult,[3,a)] and Nathaniel J. Fisch[4]

AFFILIATIONS

[1]Andlinger Center for Energy + the Environment, Princeton University, Princeton, New Jersey 08540, USA
[2]IJCLab, Université de Paris-Saclay, Orsay 91405, France
[3]LAPLACE, Université de Toulouse, CNRS, INPT, UPS, Toulouse 31062, France
[4]Department of Astrophysical Sciences, Princeton University, Princeton, New Jersey 08540, USA

[a)]Author to whom correspondence should be addressed: renaud.gueroult@laplace.univ-tlse.fr

ABSTRACT

Very large DC and AC electric fields cannot be sustained between conducting electrodes because of volume gas breakdown and/or surface field emission. However, very large potential fields are now routinely generated in plasma structures, such as laser generated wake in unmagnetized plasmas. In magnetized plasmas, large DC fields can also be sustained and controlled perpendicular to the magnetic field, but the metallic end plates limiting the plasma, terminating the magnetic field lines, and usually providing the voltage drop feed between the field lines impose severe restrictions on the maximum field. However, it is shown that very large radial DC voltage drops can be sustained by injecting waves of predetermined frequencies and wave vectors, traveling along the azimuthal direction of an axially magnetized plasma cylinder, or by injecting fast neutral particles beams along this azimuthal direction. The large conductivity along the magnetic field lines and the small conductivity between the field lines then distribute this voltage drop. The global power balance and control parameters of wave and beam generated large DC electric fields in magnetized plasmas are identified, described, and analyzed.

I. INTRODUCTION

The quest for very large electric fields is mainly driven by the need for more compact particles accelerators, but it is also important in other fields such as (i) mass separation envisioned for nuclear waste cleanup,[1] spent nuclear fuel reprocessing,[2–7] and rare earth elements recycling,[8] (ii) advanced *E* cross *B* plasma configurations for the purpose of ions acceleration,[9–11] and (iii) thermonuclear fusion with rotating tokamak[12,13] or rotating mirrors.[14–18]

Two field configurations can sustain a DC electric field in a magnetized plasma—(i) the *Brillouin configuration* with an axial magnetic field and a radial electric field[19] and (ii) the *Hall configuration* with a radial magnetic field and an axial electric field. This last configuration is the one at work in stationary plasmas thrusters where ions are unmagnetized; the former one, where ions are magnetized, is used in mass separator devices and advanced thermonuclear traps.

This study is devoted to the class of Brillouin configurations. Brillouin type of rotating plasmas has been widely studied since the early proposal of Lehnert to take advantage of the isopotential character of magnetic field lines and surfaces to sustain a voltage drop through external biasing at the edge of a plasma column with concentric electrodes.[20–24] These rotating configurations have since then been explored both theoretically and experimentally for mass separation,[25–38] thermonuclear confinement,[14–18] and the study astrophysical phenomena in laboratory experiments.[39,40]

In this new study, rather than focusing specifically on separation or fusion applications, we will address the generic issues of the power balance and the field structure of unconventional radial electric field sustainment, with waves or neutral beams, in a cylindrical plasma shell confined in a magnetized column. We will present new promising results in terms of efficiency and control of these advanced wave and beam schemes.

Three mains principles can be considered with respect to very high electric field generation:

(i) Accelerator technologies,[41] such as electrostatic, Van de Graff type, accelerators, where metallic electrodes are charged up to create a voltage drop of typically a few MV. These DC types of devices are limited by electrons emission at metallic surfaces under high electric fields and/or breakdown of the insulating gas. Modern RF and microwave accelerators bypass this drawback of metallic surface through the use of high frequency fields and can reach far higher AC electric fields values, but even at high frequencies, metallic structures display an unavoidable electric field threshold above which massive electron emission takes place.

To address breakdown and emission problems, the use of fully ionized plasma has been put forward.

(ii) Laser–plasma accelerators bypass these problems through the use of plasma rather than metals to sustain the electric charges separation and have reached voltage gradients in the GV per meter range. The basics of such schemes is the generation of a traveling electrons–ions charge separation with the ponderomotive force of an ultrashort laser pulse acting on the electron population. Indeed, a short laser pulse of length L, described by its vector potential A, will push the electrons in the propagation direction and generate a charge separation with amplitude $q^2A^2L/2m^2c^2$,[42,43] where q and m are the electron charge and mass and c is the velocity of light. Such a charge separation, of the order of tens of μm in underdense plasmas, generates large traveling fields which then will oscillate at the electron plasma frequency ω_{pe} behind the pulse as a wake. A well-phased, well-shaped charged particle bunch, following the laser pulse, can gain energy in such a laser generated electrostatic wave.

(iii) Besides these mature conventional and advanced accelerator technologies, an overlooked physical principle can be put at work to generate large DC electric field: using a magnetized plasma in which we induce a steady state charge separation perpendicular to the magnetic field through the continuous absorption of a resonant wave or the continuous ionization of a fast neutral beam.

That a magnetic field can inhibit the relaxation of the charges separation sustaining a very large voltage drop across a magnetic field is suggested by the energy associated with both electric and magnetic fields: (i) $\varepsilon_0 E^2 V/2$ for an electric field E in a volume V and (ii) $B^2V/2\mu_0$ for a magnetic field B in a volume V. A large electric field of say 10 MV/m is associated with a density of energy (pressure) of the order of few kJ/m^3, although a typical magnetic field of say 1 T is associated with a density of energy (pressure) of the order of few MJ/m^3. This very strong ordering between magnetic and electric pressure suggests why the free charges, which are attached to the magnetic field through the cyclotron motion, can resist the tendency to relaxation and (quasi-) neutralization driven by an electric field perpendicular to the magnetic field.

The wave and beam schemes considered in this study to drive an electric field in a magnetized plasma are to be compared with the more classical scheme where a voltage drop between field lines is imposed with external voltage generators connected to the field lines edges, as illustrated in Fig. 1(a). As we will demonstrate, an important conceptual difference is that in the classical scheme, the electric field $E(z)$ has to penetrate the plasma column from the edge and is decreasing along the z axis from the left and right edges toward the center. On the other hand, wave or beam power can in principle be deposited at the center of a plasma column, as shown, respectively, in Figs. 1(b) and 1(c). In these new schemes, the maximum voltage drop, thus, occurs in the center while the minimum voltage drop is found the endplates, in contrast with the classical scheme. By allowing the electric field to be localized more inside the plasma than at the edge, with a weaker interaction with any solid material, the risk of breakdown and emission near metallic endplates are reduced, and larger values can be envisioned.

Practically, the upper limit for the amplitude of electric field generated by a laser pulse in underdense plasmas is known to be associated with the occurrence of cavitation behind the pulse. This phenomenon has been observed numerically and experimentally. On the other hand, the upper limit for the amplitude of the DC electric field generated by wave or beam power absorption in magnetized plasmas has never been explored. Moreover, the possibility to isolate this large DC electric field from the plasma facing end plate in order to avoid breakdown or electron emission has never been considered. Both of these issues are considered here. We will identify the constraint arising from the plasma (i) inherent anisotropic dissipation and (ii) finite size and then translate it into realistic conditions for large field generation, distribution, and dissipation, thus identifying upper bounds on power consumption for DC high voltage generation across magnetized plasmas. We will show that upper bounds in the GV/m range can be envisioned from the proposed models of waves and beam generation under optimal conditions, but that a few MV/m already provides the necessary conditions for the very fast supersonic rotations of a fully ionized hot plasma columns (required, for instance, in thermonuclear trap) and is accessible with wave or beam power of the order of few tens of MW.

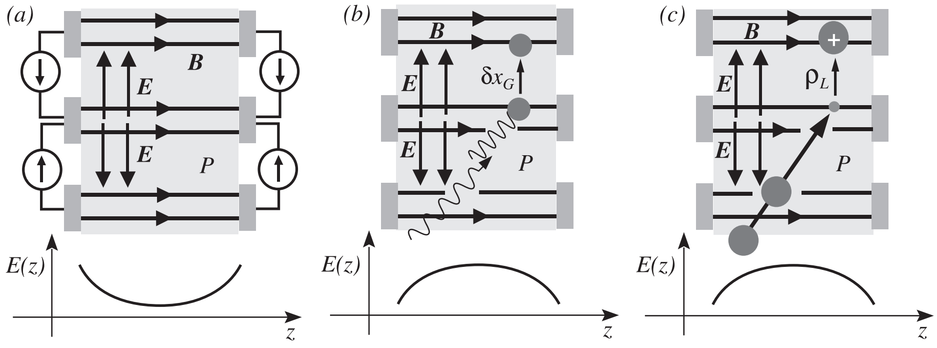

FIG. 1. (a) The classical method to sustain a perpendicular electric field in a magnetized plasma (P) column with biased edge electrodes, (b) wave driven charge separation in a magnetized plasma (P), and (c) beam driven charge separation in a magnetized plasma (P). $E(z)$ is the radial electric field between the axis and the outer cylindrical shell.

This paper is organized as follows. First, in Sec. II, we present a heuristic view of the formation of a voltage drop using waves and beams and address the issue of dissipation in a magnetized plasma. Then, in Sec. III, we briefly review the principle of charge transport driven by resonant waves in a magnetized plasma and identify from these results an upper bound for DC electric field wave driven generation. Then, in Sec. IV, we describe the principle of charge separation driven by fast neutral beam injection. The expression of the sustained DC electric field is established through three different methods giving the very same result. The order of magnitude of the maximum achievable electric field through this method is also estimated. The steady state balance between wave/beam driven charge separation/generation and dissipative charge dispersion and (quasi-) neutralization is considered in Sec. V. Specifically, a steady state model is obtained by considering the balance between (i) wave/beam driven charge separation/generation, (ii) fast distribution/spreading along the field lines, and (iii) slow relaxation across the field lines. This model is then solved in Sec. VI to identify both the plasma resistance R and the attenuation length λ, which describe the steady state of a wave, or beam, driven magnetized and polarized plasma slab. The results are then used to address in Sec. VII the issue of finite size plasmas in the case where the attenuation length is too long to ensure a good confinement of the electric field near the wave or beam active plasma zone and away from the plasma edges. We show that a decrease in the voltage drop at the edge of the plasma can be achieved at the cost of a certain loss of the efficiency of the generating process. Finally, the last section, Sec. VIII, summarizes our new findings and points toward the optimization of these DC electric field generation and confinement schemes when additional constraints are considered, either for thermonuclear control in rotating mirrors or mass separation purposes.

II. FORMATION OF VOLTAGE DROP INSIDE A MAGNETIZED PLASMA

This section provides a heuristic presentation of the problem of electric field generation in a plasma.

Consider a magnetized plasma and a Cartesian set of coordinates (x, y, z) and a Cartesian basis $(\mathbf{e}_x, \mathbf{e}_y, \mathbf{e}_z)$. A wave propagating along the y direction, perpendicular to the magnetic field $B\mathbf{e}_z$, with wave vector $k_\perp \mathbf{e}_y$ and frequency ω, generates a charge separation of the resonant population and pushes each resonant particle by an amount

$$\delta x_G = \frac{k_\perp}{q\omega B}\delta\mathcal{E}, \tag{1}$$

where $\delta\mathcal{E}$ is the amount of energy absorbed by the resonant particle and x_G is its guiding center position. This process is illustrated in Fig. 2(b).

When the quantum of energy $\delta\mathcal{E} = \hbar\omega$ is absorbed, the quantum of perpendicular momentum $\hbar k_\perp$ along y is also absorbed and, through a continuous absorption, this provides a secular force $\hbar k_\perp/\delta t$, which drives a drift along x: $\hbar k_\perp/\delta t q B$. During a time δt, the shift in position is, thus, equal to $\hbar k_\perp/qB$, which eliminating $\hbar = \delta\mathcal{E}/\omega$ gives Eq. (1). This relation, Eq. (1), will be reviewed in Sec. III.

If, rather than $\delta\mathcal{E}(\mathrm{J})$, we consider a stationary (density of) power absorption $P_{RF}(\mathrm{W/m^3})$, then Eq. (1) shows that a continuous wave drive will generate a continuous guiding center current density $J_\perp \mathbf{e}_x$ perpendicular to the magnetic field

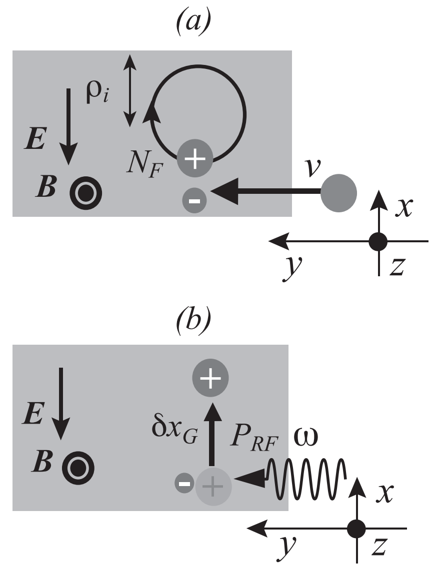

FIG. 2. (a) Neutral beam driven perpendicular electric polarization and (b) wave driven perpendicular electric current generation.

$$J_\perp\left[\frac{\mathrm{A}}{\mathrm{m}^2}\right] = \frac{k_\perp}{\omega B}\cdot P_{RF}\left[\frac{\mathrm{W}}{\mathrm{m}^3}\right], \tag{2}$$

where P_{RF} is the density of power absorbed by the resonant population. This perpendicular drift current generation has been proposed to confine toroidal plasmas[12,13] and, for unstable waves, to provide a free energy extraction mechanism from thermonuclear plasmas through *alpha channeling* in both tokamaks and mirrors.[16,44–47]

Rather than a wave, we consider now a fast neutral beam as a momentum source, with velocity $v\mathbf{e}_y$, injected in a magnetized plasma as illustrated in Fig. 2(a). When a fast neutral particle is ionized inside the plasma, the electron and the ion rotate in the opposite direction and the value of their Larmor radius is so different that these two charges are separated on average by an amount

$$\rho_i \approx \frac{Mv}{qB} \gg \rho_e, \tag{3}$$

creating an electric dipolar moment $q\rho_i$, where $\rho_{e/i}$ is the electron/ion Larmor radius and M and q are the ion mass and charge.

The balance between the ionization rate of the fast neutral and the slowing down of the fast ions provides a steady state density of fast ions N_F. The associated steady state charge separation can be described by an electric polarization $P_\perp \mathbf{e}_x$ perpendicular to the magnetic field

$$P_\perp\left[\frac{\mathrm{C}}{\mathrm{m}^2}\right] = \frac{Mv}{B}\cdot N_F\left[\frac{1}{\mathrm{m}^3}\right]. \tag{4}$$

This electric polarization $P_\perp$ is the source of a voltage drop between magnetic field lines, which will be analyzed in Sec. IV.

In this study, we will identify, describe, and analyze schemes to use this wave driven current $J_\perp$ Eq. (2) or this beam driven polarization $P_\perp$ Eq. (4) to generate a large voltage drop across the magnetic field lines in the core of the plasma. Core generation provides a way to mitigate breakdown and/or emission at the edge of the plasma when both the plasma and the field lines encounter the end plates.

A picture of the build-up phase of a growing electric field in a plasma slab can be described as follows. Note that in the following model, we do not consider the interplay between the adiabatic and resonant response of the particles[48–50] and consider the final global momentum balance. A wave, or a neutral beam, moves some minority charges across the magnetic field as shown in Eqs. (1) and (3) and, thus, sets up a current $\mathbf{J}_0(t)$ such that $\mathbf{J}_0(t=-\infty)=\mathbf{0}$ and $\mathbf{J}_0(t=0)=\mathbf{J}_0$ (dissipation is switched off for $t<0$). From an electrical point of view, this phase corresponds to a capacitive electric field build up in a non-dissipative dielectric media: the charging of a capacitor. The plasma, which displays a low frequency permittivity $\varepsilon = 1+\omega_{pi}^2/\omega_{ci}^2 \approx \omega_{pi}^2/\omega_{ci}^2$, adjusts an electric field $\mathbf{E}(t)$ such that the electrostatic limit of Maxwell–Ampère equation is fulfilled,

$$\varepsilon_0 \frac{\omega_{pi}^2}{\omega_{ci}^2}\frac{\partial \mathbf{E}}{\partial t} + \mathbf{J}_0(t) = \mathbf{0}. \tag{5}$$

It must be stressed that $\mathbf{J}_0(t)$ is here a function of all the other plasma, wave, or beam parameters and, in particular, of the DC electric field. From a mechanical point of view, this build-up phase corresponds to a momentum input through the $\mathbf{J}_0(t)\times\mathbf{B}$ force and this momentum ends up in the plasma E cross B drift, guaranteeing momentum conservation

$$\int_{-\infty}^{0} \mathbf{J}_0(t)\times\mathbf{B}dt + N_p M\frac{\mathbf{E}_0\times\mathbf{B}}{B^2} = \mathbf{0}, \tag{6}$$

where $\mathbf{E}(t=0)=\mathbf{E}_0$, M is the ion mass, and N_p is the ion density. The physical interpretation of Eq. (6) is simply that the charge accumulation described by the time integral of the current, in the first term, is the source of the electric field multiplied by the dielectric constant of the plasma, in the second term, i.e., Maxwell–Gauss's equation is fulfilled.

Then, for $t>0$ that is in the steady state dissipative regime, the charge separation associated with $\mathbf{J}_0$ is short circuited by the plasma conductivity through the conduction current $\mathbf{J}_{\text{conduction}}$ in the magnetized plasma, as well as the boundary condition at the edge of the magnetic field lines. After this build-up phase, the steady state is reached when

$$\nabla\cdot(\mathbf{J}_0+\mathbf{J}_{\text{conduction}}) = 0. \tag{7}$$

This steady state regime will be described within a framework where the plasma is modeled as a slab of an anisotropic conductor, and the end plates at the outer edges of the magnetic field lines will be modeled by a resistive load R_L.

Consider the magnetized plasma slab illustrated in Fig. 3, with the following dimensions: a along x, b along y, and l along z. This plasma slab is magnetized along z, $\mathbf{B}=B\mathbf{e}_z$, and we assume that a wave or beam driven steady state electric current I_0 flows along the face S_1 from the lower magnetic surface S_2 up to the upper magnetic surface S_3. The two magnetic surfaces S_2 and S_3 are, thus, charged like a capacitor, but the electric conductivity along the magnetic field line $\eta_\parallel$ and across the magnetic field line $\eta_\perp \ll \eta_\parallel$ complexifies this simple capacitor charging model and relaxes the stored charges. This conductive charge redistribution and relaxation are the source of the voltage distribution and power dissipation involved in the process of wave or beam DC electric sustainment in a plasma identified and analyzed here.

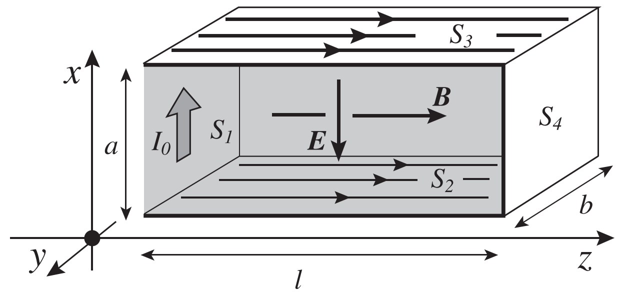

FIG. 3. A magnetized plasma slab (a, b, l) with wave or beam current drive I_0 localized on the left side S_1.

The voltage drop along S_1 between S_2 and S_3 is V_0 so that the power needed to sustain the steady state electric field $(V_0/a)\,\mathbf{e}_x$ near S_1 is simply I_0V_0. Two asymptotic cases can be considered in order to set up an equivalent circuit model.

First, if S_4 is a conductive short circuit between S_2 and S_3, the power $\mathcal{P}$ needed to sustain the steady state will be approximately

$$\mathcal{P}_{\text{short cicuit}} = I_0V_0 \approx \frac{l}{ab\eta_\parallel}I_0^2 = \frac{ab}{l}\eta_\parallel V_0^2 \tag{8}$$

as it is the conductivity along the magnetic field, which will ensure preferentially the charge relaxation at S_4. Second, if S_4 is non-conductive, S_2 and S_3 are isolated and the power needed to sustain the steady state will be approximately

$$\mathcal{P}_{\text{open cicuit}} = I_0V_0 \approx \frac{a}{bl\eta_\perp}I_0^2 = \frac{bl}{a}\eta_\perp V_0^2, \tag{9}$$

as the charge relaxation takes place across the magnetic field in the plasma volume rather than at the edge.

For a given voltage requirement V_0, and because $\eta_\perp \ll \eta_\parallel$, $\mathcal{P}_{\text{open cicuit}} \ll \mathcal{P}_{\text{short cicuit}}$. In between these two asymptotic limits, we will calculate the equivalent resistance of the slab R_e, Eq. (57), and the power balance of the wave or beam generation process, Eq. (61). These are the main new results presented in this article. The new expression for R_e involves both what we call the plasma resistance R and a penetration length λ describing the spatial decay of the voltage drop away from the source region.

III. WAVE-DRIVEN RESONANT CHARGE SEPARATION

In this section, we derive the relations, Eqs. (1) and (2), and briefly review the main relations describing the dynamics of wave driven resonant charges separation in a plasma. This phenomenon has been proposed to provide free energy extraction in thermonuclear plasmas[44–47] and to help toroidal confinement in tokamak.[12,13]

The Cartesian plasma slab considered in the following is magnetized along z, $\mathbf{B}=B\mathbf{e}_z$ and polarized along x, $\mathbf{E}=-E\mathbf{e}_x$. A wave with wave vector $\mathbf{k}=k_\perp\mathbf{e}_y+k_\parallel\mathbf{e}_z$ and frequency ω propagates in this plasma along (z) and across (y) the magnetic field. We restrict the following argument to an unspecified components of this wave oscillating with the phase $(\omega t - k_\perp y - k_\parallel z)$. In order to identify the wave-particle resonances, we plug into the phase of this wave the unperturbed motion of a charged particle characterized by the invariants $(x_G, v_\parallel, v_c)$,

$$x = x_G + \frac{v_c}{\omega_c}\cos(\omega_c t), \tag{10}$$

$$y = \frac{E}{B}t + \frac{v_c}{\omega_c}\sin(\omega_c t), \tag{11}$$

$$z = v_\parallel t. \tag{12}$$

Here, ω_c is the cyclotron frequency, v_c is the cyclotron velocity, $v_\parallel$ is the velocity along the field lines, and x_G is the guiding center position along x. The phase seen by a particle is, thus,

$$\cos\left(\omega t - k_\perp y - k_\parallel z\right) \sim \cos\left(\omega t - k_\perp \frac{E}{B}t - k_\perp \frac{v_c}{\omega_c}\sin\omega_c t - k_\parallel v_\parallel t\right). \tag{13}$$

This result can be rearranged with the classical Euler Bessel expansion

$$\cos(a + b\sin\phi) = \sum_{N=-\infty}^{N=+\infty} \mathrm{J}_N(b)\sin(a + N\phi), \tag{14}$$

so that the field seen by the particle becomes a series of harmonics with Bessel function amplitudes

$$\cos\left(\omega t - k_\perp y - k_\parallel z\right) \sim \sum_{N=-\infty}^{N=+\infty} \mathrm{J}_N\left(k_\perp \frac{v_c}{\omega_c}\right) \times \sin\left(\omega t - k_\perp \frac{E}{B}t - N\omega_c t - k_\parallel v_\parallel t\right). \tag{15}$$

Thus, a resonance might occur with the N component of this spectral expansion if this oscillating amplitude becomes stationary

$$\omega - k_\perp E/B - N\omega_c - k_\parallel v_\parallel = 0. \tag{16}$$

When this condition is fulfilled, the topology of the particles motion phase portrait changes and particles trapped in the wave experience a large variation of the invariants of the free motion $(x_G, v_\parallel, v_c)$. When this condition is not fulfilled, the particles oscillate and this oscillation is associated with a reactive power so that no active power is exchanged with non-resonant (adiabatic) particles.

For such resonances, if an amount $\delta\mathcal{E}$ of RF energy is absorbed by a resonant particle, then the unperturbed motion invariants $(x_G, v_\parallel, v_c)$ are no longer invariant. Because of the resonant interaction with the wave they become $(x_G + \delta x_G, v_\parallel + \delta v_\parallel, v_c + \delta v_c)$ where $(\delta x_G, \delta v_\parallel, \delta v_c)$ are proportional to $\delta\mathcal{E}$, a simple dynamical analysis allows us to write the set of relations as follows:

$$\delta x_G = \frac{k_\perp}{q\omega B}\delta\mathcal{E}, \tag{17}$$

$$m\delta v_\parallel = \frac{k_\parallel}{\omega}\delta\mathcal{E}, \tag{18}$$

$$m v_c \delta v_c = N\frac{\omega_c}{\omega}\delta\mathcal{E}. \tag{19}$$

Equation (17) is associated with the conservation of the canonical momentum along y. Equation (18) is associated with the conservation of classical momentum along z. Finally, Eq. (19) describes harmonic cyclotron heating. These relations can be rederived from an Hamiltonian analysis[51] or simply from the quantum photon picture described in Sec. II.

Global (wave + particle) energy conservation can be simply checked as follows. The complete variation of a resonant particle kinetic $mv_\parallel \delta v_\parallel + mv_c\delta v_c$ and potential $qE\delta x_G$ energy is

$$qE\delta x_G + mv_\parallel\delta v_\parallel + mv_c\delta v_c = \frac{\delta\mathcal{E}}{\omega}\left(\frac{k_\perp E}{B} + k_\parallel v_\parallel + N\omega_c\right) = \delta\mathcal{E}, \tag{20}$$

where we have used the resonance condition Eq. (16) to obtain the final identity.

From these results, we can identify a theoretical maximum electric field E^* that can be sustained *in situ* in a plasma with this type of resonant charge separation process. The optimal wave such that all the energy $\delta\mathcal{E}$ goes to the charge separation and ends up in the form of potential, $qE\delta x_G$, rather than kinetic, $mv_\parallel\delta v_\parallel + mv_c\delta v_c$, energy, is a wave displaying no Landau and cyclotron absorptions such that $k_\parallel = N = 0$ (we do not consider here anomalous Doppler resonances where the wave transfers energy between degrees of freedom). Equation (16), thus, becomes a simple drift resonance: $\omega = k_\perp E^*/B$. This last relation is confirmed by the energy balance restricted to potential energy $\delta\mathcal{E} = qE^*\delta x_G$. Then, with the help of Eq. (17), we eliminate $\delta\mathcal{E}$ to find the constraint on the DC electric field E^*_{RF},

$$\frac{E^*_{RF}}{B} = \frac{\omega}{k_\perp}. \tag{21}$$

Very large E^*_{RF} can, thus, in principle be reached for very large B field values, though it is to be noted that the wave dispersion $\omega(k_\perp)$ is also a function of B. Taking a moderate value of B of the order of few tesla and a high frequency wave with a velocity of the order of the velocity of light, which is the case in tenuous plasmas, we end up with electric fields values of the order of 1 GV/m. The relation Eq. (21), however, only offers a partial view of the problem because if we want to drive the plasma drift motion we need waves with a large momentum $k_\perp$, whereas Eq. (21) suggests that small $k_\perp$ are preferable for large electric field. Equation (21) is an upper bound associated with an optimal use of the wave power in term of efficiency. It is a kinematical constraint associated with optimal resonance. This large value is only achieved if dissipation (charges relaxation) is neglected. In the following, we will assume that the wave driven charge separation takes place in a narrow region around $z = 0$ and that this RF region is hot and collisionless but the neighboring region is assumed collisional, and we will analyze the impact of dissipative charge relaxation in a plasma slab.

IV. NEUTRAL-BEAM-DRIVEN CHARGE SEPARATION

In this section, we derive the relations Eqs. (3) and (4) and set up and solve a simple model describing beam driven charges separation and electric field generation in a magnetized plasma. This phenomena is illustrated in Fig. 2(a): a beam of fast neutral atoms with velocity $v\mathbf{e}_y$ and density N_B is directed toward a plasma magnetized with $\mathbf{B} = B\mathbf{e}_z$. These fast atoms are ionized through collisions with the plasma electrons and ions and also through charges exchange with slow ions. Both processes provide fast ions generation from these fast neutral.

The rate of fast ion generation from fast neutral is ν, and it takes into account both ionization and charge exchange. As soon as a fast ion is generated in the plasma, it starts to slow down with a typical slowing down time τ. If we consider fast hydrogen atom in a thermonuclear $pB11$ plasma, τ also accounts for fast proton pitch angle scattering on boron ions. A full model of momentum transfer with neutral beam was introduced by Putvinskii in Ref. 52, addressing, in particular, the saturation of the momentum exchange when the beam velocity becomes of the order of the plasma velocity. Here, in order to identify the basic scaling with respect to the beam power at low power, we present a simple model valid in the limit that $v \ll E/B$. The density of fast ions in the plasma, N_F, is, thus, given by the solution of the particles balance,

$$\frac{dN_F}{dt} = \nu N_B - \frac{N_F}{\tau}. \tag{22}$$

Considering a steady state injection, the relation between the density of fast ions, i.e., ions with a large Larmor radius, and the density of injected neutral is

$$N_F = N_B \nu \tau. \tag{23}$$

Three methods are considered below to calculate the DC electric field sustained by steady state neutral beam injection.

First, the conservation of linear momentum in the y direction can be used to calculate the electric field $E\mathbf{e}_x$ generated by the beam. If we neglect the electron mass m in front of the ion mass M, the beam density of momentum $N_B M v$, which is coupled to the plasma at a rate ν, provides a density of force $N_B M v \nu$. This density of force acts during a time τ on the plasma. The corresponding density of momentum $N_B M v \nu \tau \mathbf{e}_y$ is absorbed in the form of plasma linear momentum along y. If we write N_P the plasma density, the linear momentum balance can be written as

$$N_B M v \nu \tau \mathbf{e}_y = N_p M \frac{E\mathbf{e}_x \times B\mathbf{e}_z}{B^2}. \tag{24}$$

The very same relation can be obtained from an electrical analysis rather than from a mechanical point of view. If we neglect the electron Larmor radius in front of the ion Larmor radius, the steady state density of fast ions N_F is associated with an electric polarization Eq. (4) $N_F q \rho_i \mathbf{e}_x = N_F (Mv/B)\mathbf{e}_x$. In response to this electric polarization, the plasma, which displays a low frequency permittivity $\varepsilon = 1 + \omega_{pi}^2/\omega_{ci}^2 \approx \omega_{pi}^2/\omega_{ci}^2$, sets up a reverse polarization through an electric field generation $E\mathbf{e}_x$. The condition for this dielectric dipole screening is

$$N_F \frac{Mv}{B}\mathbf{e}_x + \varepsilon_0 \frac{\omega_{pi}^2}{\omega_{ci}^2} E\mathbf{e}_x = \mathbf{0}. \tag{25}$$

Here, ω_{pi} is the ion plasma frequency and ω_{ci} is the ion cyclotron frequency. Taking the cross product of this last relation with $\mathbf{B}$, we find the condition

$$-N_B \nu \tau M v \mathbf{e}_y + M N_p \frac{E\mathbf{e}_x \times B\mathbf{e}_z}{B^2} = \mathbf{0}, \tag{26}$$

which is Eq. (24).

Finally, as a third demonstration of this result, we can consider Maxwell–Ampère equation with (*i*) the polarization current $d\mathbf{P}_\perp/dt = (N_B M v/B)\nu \mathbf{e}_x$, describing the generation of fast ions and (*ii*) the displacement current $\varepsilon_0 \varepsilon \partial \mathbf{E}/\partial t = \varepsilon_0 \varepsilon \mathbf{E}/\tau$ associated with the decay of the electric field due to these fast ions slowing down. In writing Maxwell–Ampère equation, we neglect the diamagnetic effect of the fast ions and consider $\mathbf{B}_{fastions} = \mathbf{0}$ such that $\nabla \times \mathbf{B}_{fastions} = \mathbf{0}$, which implies $\partial \mathbf{P}_\perp/\partial t + \varepsilon_0 \varepsilon \partial \mathbf{E}/\partial t = \mathbf{0}$. In this case,

$$N_B \frac{Mv}{B} \nu \mathbf{e}_x + \varepsilon_0 \frac{\omega_{pi}^2}{\omega_{ci}^2} \frac{E}{\tau} \mathbf{e}_x = \mathbf{0}, \tag{27}$$

which is again identical to Eqs. (24) and (26).

Thus, no matter the point of view, (i) mechanical with the momentum balance Eq. (24), (ii) electrostatic with the dielectric dipole screening Eq. (26), and (iii) electrodynamic with Maxwell–Ampère Eq. (27), we find that the continuous injection of a neutral beam along y will sustain a DC electric field along x,

$$\frac{E_{NB}}{B} \simeq v \min\left(1, \frac{N_B}{N_p} \nu \tau\right). \tag{28}$$

The introduction of the upper bound $E_{NB} = vB$ in Eq. (28) comes from the fact that we assumed here as indicated earlier that the beam velocity v is much larger than the plasma drift velocity $E\mathbf{e}_x \times B\mathbf{e}_z/B^2$ in the three derivations above. Indeed, when the drift velocity approaches the beam velocity the electric field drive saturates.[52] Although this may seem restrictive, it is expected to hold in most cases of interest here. To see this one must recall that the spontaneous rotation of a plasma column with an axial magnetic field and a radial electric field is governed by the slow Brillouin mode,[19,53] and the angular rotation frequency is, thus, limited to fraction of the ion cyclotron frequency. This separation between plasma angular rotation and ion cyclotron should be even larger when considering that faster rotations, meaning closer to the Brillouin limit, are likely to lead to instabilities.[54–56] The desirable operating regime, thus, corresponds to $\omega_{ci}^{-1}|E/(Br)| \ll 1$. For magnetic fields of a few Teslas, the ion cyclotron frequency of boron ions or alphas is about a few tens of MHz, which for a device that is a few meters in radius then gives a maximum drift velocity of about 10^6 m s^{-1}. For a proton, this is at most a few keV that is well below typical neutral beam energies. This ordering *a posteriori* supports the hypothesis that we made to get Eqs. (24), (26), and (27), and from there Eq. (28).

Let us finally estimate Eq. (28) for plasma parameters typical of large tokamak plasmas experiments $N_B/N_p \sim 10^{-4}$–10^{-5}, $\nu\tau \sim 10^5$–10^6 and $v \sim 10^6$–10^7 (m/s). In all these relations, both ν and τ are averaged values as they are functions of the neutrals and fast ions velocities. Since in this case $\nu\tau N_B/N_p$ is comparable or larger than 1, we find an upper bound of tens of MV/m for the DC electric field generation driven by a neutral beam in a magnetized plasma with a magnetic field of a few Teslas.

V. VOLTAGE DROP DISTRIBUTION IN A PLASMA

The results obtained in Secs. III and IV suggest that both waves and neutral beams can drive perpendicular electric fields as large as a few MV/m, and likely even larger for wave drive. Because such fields are typical of advanced high energy supersonic rotating plasmas applications, we consider now the full picture by addressing the complementary issues of voltage distribution and dissipation in the bulk of a finite size plasma slab, far from the wave or beam active regions.

Consider for this a cylindrical plasma shell uniformly magnetized along the z axis. In addition to the axial magnetic field $\mathbf{B} = B\mathbf{e}_z$, we consider a radial electric field generated in a cylindrical shell of magnetic field lines, with width a and radius $b/2\pi$, depicted in gray in Fig. 4(a). The radial electric field is generated in this cylindrical shell to

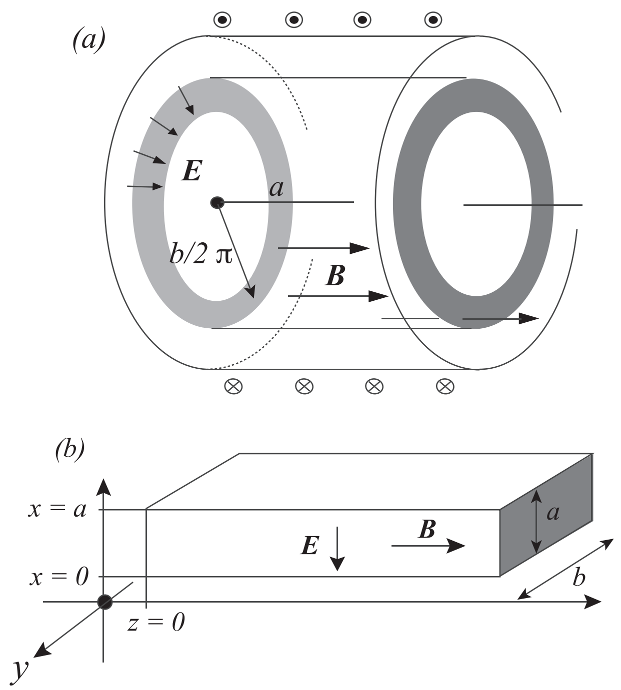

FIG. 4. Geometrical characteristics of the Cartesian plasma slab (b) modeling the cylindrical plasma shell (a).

sustain a rotation around the z axis for the purpose of thermonuclear confinement or mass separation.

In order to simplify the analysis, which can be also carried in cylindrical coordinates, we will neglect curvature effects ($b > a$) and describe the gray plasma zone of Fig. 4(a) as a slab plasma depicted in Fig. 4(b). This transformation is just an unfolding of the cylindrical shell and displays the advantage of simplifying the physical picture and results. Following this unfolding, the Cartesian plasma slab considered in the following is both magnetized along z, $\mathbf{B} = B\mathbf{e}_z$, and polarized along x, $\mathbf{E} = -E\mathbf{e}_x$.The magnetized plasma slab is of finite size: (*i*) a along x, (*ii*) b along y, and (*iii*) l along z, as illustrated in Fig. 5(b).

The electric field is described by an electrostatic potential V such that $\mathbf{E} = -(\partial V/\partial x)\mathbf{e}_x - (\partial V/\partial z)\mathbf{e}_z$, where $\partial V/\partial z < \partial V/\partial x = V/a$. The equivalent DC current generator (wave or beam), located

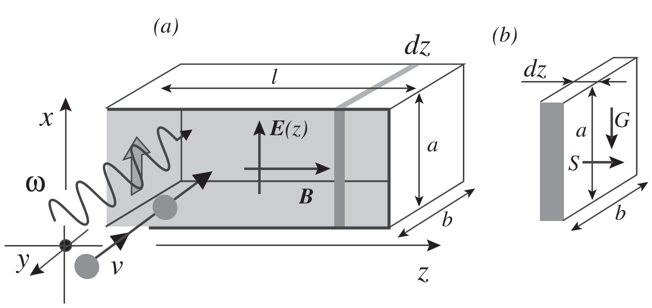

FIG. 5. (a) A plasma slab magnetized along z and polarized along x through wave/beam power absorption at $z = 0$. (b) An infinitesimal slice dz is fully characterized by its transverse conductance Gdz and longitudinal resistance Rdz.

at $z = 0$, sustains a current between $x = 0$ and $x = a$. As a result of charges depletion at $x = 0$ and charges accumulation at $x = a$, a voltage drop $V_0 = V(z = 0)$ is sustained between the magnetic surfaces $x = 0$ and $x = a$. This voltage drop will decay away for $z > 0$ because of the finite conductivities along z and across x. These finite conductivities will provide a fast dispersion of the charges along z and a slow relaxation across **B** along x.

We assume (*i*) that the amplitude of the wave is shaped such that the wave equivalent current generator is driven from $x = 0$ up to $x = a$ near $z = 0$ and (*ii*) that the density of the neutral beam is shaped such that the beam equivalent voltage generator sets up a voltage drop between $x = 0$ and $x = a$ near $z = 0$. In order to describe dissipative processes in the slab $z > 0$, we consider an infinitesimal slice of magnetized plasma: dz along z, a along x, and b along y. This elementary slab, depicted in Fig. 5(b), displays two properties: (i) a large conductivity along dz and (ii) a large resistivity along x. We assumed cylindrical symmetry of the original problem which translates into homogeneity along y of the unfolded slab. In particular, as the wave and beam travel in the y direction, we assume homogeneous wave or beam power deposition along y near $z = 0$, which means homogeneous current generation and electric field generation along y.

We describe the dissipative dynamics of the charges by the current $I(z)$, which flow easily along z and the small short circuited current resulting from the small conductivity along x. In a slice dz, this short circuiting of the initial charges separation is described by dI/dz. This model allows to describe the volume charges relaxation and the steady state large voltage drop generation across the magnetic field. To calculate the small conductivity Gdz along x (across B) and the small resistivity Sdz along z (along B), we apply the classical formula describing the resistance/conductance of the elementary parallelepiped depicted in Fig. 5(b),

$$Sdz = \frac{dz}{\eta_\parallel ba}, \tag{29}$$

$$Gdz = \frac{\eta_\perp bdz}{a}, \tag{30}$$

where we have introduced the classical conductivities $\eta_\parallel$ and $\eta_\perp$ along and across the field lines in a magnetized plasma.[57–62] Note that taking into account curvature effects would change the expression of G but not S, with for the cylindrical shell illustrated in Fig. 4(a),

$$G = 2\pi\eta_\perp \Big/ \ln \frac{1 + (\pi a/b)}{1 - (\pi a/b)}, \tag{31}$$

and we recover the previous expression if $a \ll b$. Then, we apply Ohm's law to the transmission line like model illustrated in Fig. 6(a) to write the equations fulfilled by the voltage V across x and the current I along z,

$$dV = -SIdz, \tag{32}$$

$$dI = -GVdz. \tag{33}$$

In order to obtain the various scalings and order of magnitude estimates of the final results, we use the classical formula for the longitudinal and transverse conductivities used in Eqs. (29) and (30).

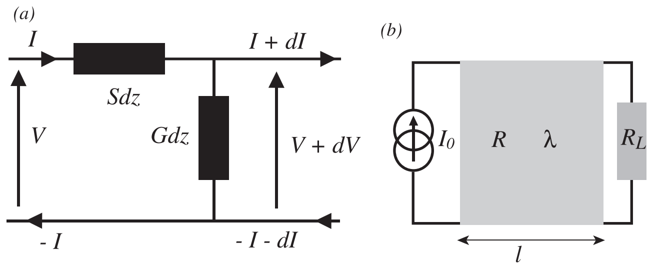

FIG. 6. (a) Equivalent circuit of a (a, b, dz) slice of the plasma. (b) Equivalent model of power absorption and charge separation near $z = 0$ and charge distribution in the plasma slab terminated with loaded endplates at $z = l$.

Assuming first that the plasma is not fully ionized and that collisions with neutrals at rest are the dominant dissipative process,

$$\eta_{\parallel} = \frac{n_m q^2}{m\nu_m}, \quad \eta_{\perp} = \frac{n_M Q^2 \nu_M}{M\omega_c^2}. \tag{34}$$

Here, n is the density of free charges with mass m (electrons) or M (ions) and charges q or Q, $\eta_{\parallel}$ is associated with the electron population and $\eta_{\perp}$ with the ion one, and $n_M Q = n_m q$. The collision frequency ν can be either the collision frequency with neutrals in a cold plasma or the turbulent decorrelation frequency in a turbulent plasma.

On the other hand, if the plasma is fully ionized, the conductivity along the field lines is given by the Spitzer conductivity. It is independent of the density but scales as $T^{-3/2}$ with the temperature,

$$\eta_{\parallel} = \varepsilon_0 \frac{\omega_{pe}^2}{\nu_{ei}}. \tag{35}$$

Across the field lines, no relative velocity between electrons and ions is observed in the $\mathbf{E} \times \mathbf{B}$ rest frame. This means that we have to consider an additional effect to find a dissipative channel. Among these processes, (*i*) inertia, (*ii*) viscosity, and (*iii*) inhomogeneity are usually put forward.[25,26,63] A clear discussion of the various regimes of dissipation across magnetic field lines can be found in Ref. 63. Here, we will consider the effect of inhomogeneity, which displays the same scaling as viscosity.[63] In an inhomogeneous electric field, the expression of the electric drift velocity $\mathbf{v}_{E\times B}$ is given by

$$\mathbf{v}_{E\times B} = \left(1 + \frac{\rho^2}{4}\frac{d^2}{dx^2}\right)\frac{\mathbf{E}\times\mathbf{B}}{B^2}, \tag{36}$$

where ρ is the Larmor radius. We will assume $d^2E/dx^2 \sim E/a^2$. This velocity is along y and, because of the difference in Larmor radius $\rho_e \ll \rho_i$, Coulomb collisions, at a rate ν_{ie}, provide a friction force F between the electron and ion populations. As a result, the ion population experiences an y directed force F,

$$F = \nu_{ie}\frac{k_B T_i}{4\omega_{ci}^2}\frac{E}{a^2 B}, \tag{37}$$

where ω_{ci} is the ion cyclotron frequency. This force F along y is the source of a $\mathbf{F}\times\mathbf{B}/QB^2$ drift along x, and this drift gives the equivalent conductivity $\eta_{\perp}$ associated with inhomogeneity

$$\eta_{\perp} = n_i \frac{\nu_{ie}}{\omega_{ci}}\frac{\rho_i^2}{a^2}\frac{Q}{4B} = \frac{\varepsilon_0}{4}\nu_{ie}\frac{\omega_{pi}^2}{\omega_{ci}^2}\frac{\rho_i^2}{a^2}. \tag{38}$$

The strong scaling with respect to the magnetic field $\rho_i^2/\omega_{ci}^2 \sim B^{-4}$ is to be noted. The effect of viscosity displays the same scaling, and we will consider Eq. (38) as the approximate perpendicular conductivity of a fully ionized plasma.[63] In the following, to evaluate the power dissipation with Eqs. (35) and (38), we will use the following estimate for a fully ionized hydrogen plasma:

$$\nu_{ei} = \ln\Lambda\left[\frac{mc^2}{3k_B T}\right]^{\frac{3}{2}}\frac{r_e}{c}\omega_{pe}^2 \sim \left[\frac{mc^2}{3k_B T}\right]^{\frac{3}{2}}\left[\frac{\omega_{pe}}{10^{11}\,\mathrm{Rd/s}}\right]^2, \tag{39}$$

where $r_e = 2.8 \times 10^{-15}$ m is the classical electron radius, $mc^2 = 511$ KeV is the electron rest energy, and $c = 2.9 \times 10^8$ m/s is the velocity of light. The ion–electron collision frequency is given by $\nu_{ie} = m\nu_{ei}/M$.

VI. ATTENUATION LENGTH AND PLASMA RESISTANCE

In order to analyze Eqs. (32) and (33), it turns out to be more convenient to introduce what we will call the *plasma slab resistance R* defined as

$$Rb = \frac{1}{\sqrt{\eta_{\perp}\eta_{\parallel}}}, \tag{40}$$

and the *attenuation length* λ defined as

$$\frac{\lambda}{a} = \sqrt{\frac{\eta_{\parallel}}{\eta_{\perp}}}. \tag{41}$$

These two global characteristics, R and λ, capture all the electrical properties of the plasma slab needed to describe the charge relaxation for $z > 0$ of the $z = 0$ wave or beam driven perpendicular current.

For a fully ionized plasma, the transverse conductivity is a second order effect described in Eq. (38), and the plasma resistance and attenuation length are given by

$$\frac{\lambda}{a} = \frac{2}{\sqrt{\nu_{ei}\nu_{ie}}}\frac{\omega_{pe}\omega_{ci}}{\omega_{pi}}\frac{a}{\rho_i} \sim \frac{\omega_{ci}}{\nu_{ie}}\frac{a}{\rho_i}, \tag{42}$$

$$\frac{1}{Rb} = \frac{\varepsilon_0}{2}\frac{\omega_{pe}\omega_{pi}}{\omega_{ci}}\sqrt{\frac{\nu_{ie}}{\nu_{ei}}}\frac{\rho_i}{a} \sim \varepsilon_0\frac{\omega_{pe}^2}{\omega_{ce}}\frac{\rho_i}{a}. \tag{43}$$

The attenuation length λ is, thus, far larger than the size of the device for a fully ionized plasma of the thermonuclear type. Note also that while the definition of the attenuation length λ, Eq. (41), already appears in the literature in the few studies addressing the issue of field penetration from the edge,[59,60,62] the definition of

$$R = \frac{\omega_{ce}a}{b\varepsilon_0\rho_i\omega_{pe}^2}$$

for a fully ionized plasma, Eq. (43), does not seem to have attracted some previous specific attention despite its importance to understand DC voltage distribution in a fully ionized magnetized plasma.

With these definitions, Eqs. (32) and (33) become simply

$$\lambda\frac{dV}{dz} = -RI, \tag{44}$$

$$\lambda\frac{dI}{dz} = -\frac{V}{R}. \tag{45}$$

We further define the new variables $s = z/\lambda$ and (u, v) such that

$$\begin{pmatrix} u \\ v \end{pmatrix} = \begin{pmatrix} \dfrac{V}{\sqrt{R}} + \sqrt{R}I \\ \dfrac{V}{\sqrt{R}} - \sqrt{R}I \end{pmatrix}, \tag{46}$$

so that

$$\frac{d}{ds}\begin{pmatrix} u \\ v \end{pmatrix} = \begin{pmatrix} -u \\ +v \end{pmatrix}. \tag{47}$$

The solutions of Eq. (47) are simply a *forward decay* $u = u_0 \exp -s$ and a *backward decay* $v = v_0 \exp s$.

Note for completeness that Eq. (47) was derived by assuming that the plasma is homogeneous. A simple model taking into account the z variation of $\lambda(z)$ and $R(z)$ can be studied in a way similar to the analysis of the previous homogeneous model but by considering this time the change in variable,

$$s(z) = \int_0^z du/\lambda(u). \tag{48}$$

With this change in variables, Eq. (47) becomes

$$\frac{d}{ds}\begin{pmatrix} u \\ v \end{pmatrix} = \begin{pmatrix} -u \\ +v \end{pmatrix} - \left(d \ln \sqrt{R}/ds\right)\begin{pmatrix} v \\ u \end{pmatrix}, \tag{49}$$

and the forward and backward solutions are coupled by the inhomogeneities. This inhomogeneities $\lambda(z)$ and $R(z)$ play the role of an additional dissipative term, for example, when the magnetic field lines are diverging. Although interesting generalizations, the tapering effect of inhomogeneous plasma and magnetic field properties will not be considered here, and we will restrict the analysis to the solutions of Eq. (47).

The general solution of Eqs. (44) and (45) is a linear combination of the forward and backward solutions $\exp +z/\lambda$ and $\exp -z/\lambda$. In the following, we consider the general solution

$$I(z) = I_- \exp\left(-\frac{z}{\lambda}\right) + I_+ \exp\left(+\frac{z}{\lambda}\right), \tag{50}$$

$$V(z) = RI_- \exp\left(-\frac{z}{\lambda}\right) - RI_+ \exp\left(+\frac{z}{\lambda}\right), \tag{51}$$

where the amplitudes $I_\pm$ are given by the two boundary conditions (i) at $z = 0$ with the wave or beam driven generators, and (ii) at $z = l$ with a load R_L describing how we choose to terminate the field lines and the plasma. This is illustrated in Fig. 6(b). The $\exp +z/\lambda$ solution is associated with the reflection on the load at $z = l$ when there is an impedance mismatch of this load R_L with the plasma resistance R.

The boundary condition at $z = 0$ depends on whether wave or neutral beam is considered. For the wave case, as the effect of the wave is to move already existing charges, we consider an equivalent perfect current generator $I_0|_{RF}$ localized at $z = 0$. For the neutral beam case, as the beam brings and separates charges with opposite signs, we consider an equivalent perfect voltage generator $V_0|_{NB}$ localized at $z = 0$. We call $I_0 = I(z = 0)$ the current of the generator equivalent to the wave, and $V_0 = V(z = 0)$ the voltage drop in the beam active region near $z = 0$. These current and voltage generators can be, respectively, related to the injected RF power and beam momentum as follows.

Writing $\mathcal{P}_{RF}$[W] the total power absorbed by the plasma from the wave at $z = 0$ where the wave power deposition is localized, one gets

$$P_{RF}\left[\mathrm{W/m^3}\right] = \frac{\mathcal{P}_{RF}\delta(z)}{ab}, \tag{52}$$

where $\delta(z)$ is the Dirac distribution. Then, from Eq. (2), we can define the equivalent current generator $I_0|_{RF}$ associated with the wave drive at $z = 0$ through the relation $J_\perp = I_0|_{RF}\delta(z)/b$, so that

$$I_0|_{RF} = \frac{k_\perp}{\omega}\frac{1}{Ba}\mathcal{P}_{RF}. \tag{53}$$

Similarly, we can define from Eq. (28) the equivalent voltage generator $V_0|_{NB} = E_{NB}a$ associated with the beam drive at $z = 0$,

$$V_0|_{NB} = aB\nu\tau\frac{N_B}{N_p}v. \tag{54}$$

For the wave case, the power of the wave equivalent generators is $I_0|_{RF}V_0$. Under optimal conditions such as discussed in Sec. II, energy conservation implies that the input RF power is equal to the dissipated DC power: $I_0|_{RF}V_0 = \mathcal{P}_{RF}$. Eliminating $\mathcal{P}_{RF}$ between this last relation and Eq. (53), we recover Eq. (21) as expected.

Because of dissipation, the current $I_0|_{RF}$ and voltage $V_0|_{NB}$ are progressively shunted by the plasma, away from $z = 0$, as a result of the high conductivity along z and the weak conductivity along x. This decrease is described by the solution Eqs. (50) and (51) under the appropriate boundary conditions $I(z = 0) = I_0$ or $V(z = 0) = V_0$ given in Eqs. (53) and (54) and $V(z = l) = R_L I(z = l)$ at the end of the field lines for a plasma column of length l.

VII. POWER DISSIPATION IN A LOADED PLASMA SLAB

A. Power requirement

We consider Eqs. (50) and (51) with the wave or beam driven generator Eq. (53) or Eq. (54) at $z = 0$, and with the plasma being terminated at $z = l$ by a resistive load R_L as illustrated in Fig. 6(b). These boundary conditions can be written as

$$I_- + I_+ = I_0, \tag{55}$$

and

$$R\left(I_- \exp -\frac{l}{\lambda} - I_+ \exp +\frac{l}{\lambda}\right) = R_L\left(I_- \exp -\frac{l}{\lambda} + I_+ \exp +\frac{l}{\lambda}\right). \tag{56}$$

After some elementary algebra, we solve Eqs. (55) and (56) for the amplitudes $I_\pm$ and express $V(z = 0)$ as a function of $I(z = 0)$ through the definition of R_e: $V_0 = R_e I_0$. This resistance R_e is the equivalent resistance of the plasma slab as seen from $z = 0$ and writes

$$\frac{R_e}{R} = \frac{R_L + R\tanh l/\lambda}{R + R_L\tanh l/\lambda}. \tag{57}$$

For the wave case, Eq. (53) relates the current $I_0|_{RF}$ to the RF power $\mathcal{P}_{RF}$. This power is used to sustain the steady state current and voltage pattern in the plasma slab (a, b, l) against relaxation. The maximum voltage drop in the wave active region $z = 0$ is, thus,

$$V_0|_{RF} = R_e \frac{k_\perp}{a\omega B}\mathcal{P}_{RF} \leq \frac{R}{\tanh l/\lambda}\frac{k_\perp}{a\omega B}\mathcal{P}_{RF}, \tag{58}$$

where the right hand side of the inequality, $R_e = R/\tanh l/\lambda$, is associated with the optimal choice for the load at $z = l$, that is $R_L \to +\infty$. As $\tanh l/\lambda$ increases from zero up to one when l increases, a shorter plasma column displays a larger voltage drop for the same power because the charges are more concentrated on the field lines, in the limit that $l < \lambda$. With the expansion

$$R_e|_{R_L \to +\infty} = \frac{R}{\tanh l/\lambda} \approx \frac{\lambda R}{l} = \frac{a}{bl\eta_\perp}, \tag{59}$$

the plasma slab behaves as an isotropic conductor with conductivity $\eta_\perp$ and Eq. (58) becomes

$$V_0|_{RF} \approx \frac{k_\perp}{bl\eta_\perp \omega B}\mathcal{P}_{RF}. \tag{60}$$

Dissipation across the field lines is ultimately responsible for the limit described in Eq. (60). For such a favorable limit, even if $\eta_\perp \to 0$ or $\mathcal{P}_{RF} \to +\infty$, the optimum voltage V_0 is limited by the relation Eq. (21), which is a constraint imposed by the wave-particle resonance if we want to optimize the generation process and avoid to waste power into Landau and cyclotron heating.

Using Eq. (38), the power requirement $\mathcal{P} \sim bl\eta_\perp V_0^2/a$ for a given voltage drop and a given fully ionized plasma under optimal conditions is

$$\left[\frac{\mathcal{P}}{\mathrm{W}}\right] \sim \left[\frac{V_0}{\mathrm{MV}}\right]^2 \left[\frac{\omega_{pe}}{10^{11}\ \mathrm{rad.s^{-1}}}\right]^2 \left[\frac{l}{\mathrm{m}}\right]\left[\frac{b}{a}\right]\left[\frac{k_B T}{mc^2}\right]^{-\frac{3}{2}}\left[\frac{\rho_i}{a}\right]^2\left[\frac{\omega_{pe}}{\omega_{ce}}\right]^2, \tag{61}$$

where we assumed $\ln\Lambda = 10$. This result suggests that megavolt voltage drops are accessible for rather low driving power in thermonuclear hydrogen plasmas where typically $b \sim a$, $\omega_{pe} \sim \omega_{ce}$ and $a \geq 10\rho_i$.

Up to now we have only considered a current source (equivalent to the wave or the beam) localized near $z = 0$. For wave drive, this is true if the resonant particles are chosen with a zero parallel velocity, and/or if the plasma column is very long, and/or if the quasilinear wave diffusion from $x = 0$ to $x = a$ is fast enough compared to the other processes. This issue of the radial current deposition by a wave must be addressed within the framework of a collisional/quasilinear kinetic model. Similarly the issue of the neutral beam current deposition is to be addressed within a kinetic model. Rather than going this route, we consider here for completeness the previous fluid model but the complementary and more general problem of a broad current deposition profile. Specifically, the wave or beam current deposition is assumed to be broadly distributed all along the field lines, $0 < x < l$, and described by an infinitesimal current source, $\mathcal{I}dz = (I_0/l)dz$, in each infinitesimal section dz along z. We consider the equivalent circuit associated with an infinitesimal section dz as illustrated in Fig. 7(a). The electrical properties of a slice (a, b, dz) then take into account a $\mathcal{I}dz$ current source.

The transmission line equations describing the slab (a, b, l) with load R_L at $z = l$ as illustrated in Fig. 7(b) are

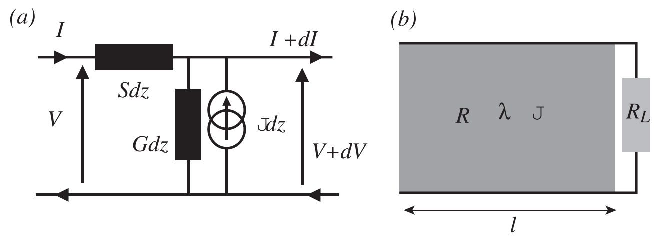

FIG. 7. (a) Equivalent circuit of a dz slice (a, b, dz) of the plasma. (b) Equivalent model of wave absorption and charge separation and charge dissipation in the plasma slab (a, b, l) terminated with loaded endplates at $z = l$.

$$\lambda\frac{dV}{dz} = -RI, \tag{62}$$

$$\lambda\frac{dI}{dz} = -\frac{V}{R} + \lambda\mathcal{I}. \tag{63}$$

Note that Eqs. (62) and (63) will still hold true if considering plasma conductivities and power deposition profiles that are inhomogeneous along z. With the boundaries conditions $I(z = 0) = 0$ and $R_L I(z = l) = V(z = 0)$, the solutions are given by

$$I(z) = \mathcal{I}\lambda\frac{R\sinh(z/\lambda)}{R\cosh(l/\lambda) + R_L\sinh(l/\lambda)}, \tag{64}$$

$$V(z) = R\mathcal{I}\lambda\left[1 - \frac{R\cosh(z/\lambda)}{R\cosh(l/\lambda) + R_L\sinh(l/\lambda)}\right]. \tag{65}$$

With these solutions, we can now define two equivalent resistances. The first one is simply the ratio of the voltage $V_0 = V(z = 0)$ to the total wave or beam driven current $I_0 = \int_0^l \mathcal{I}dz$,

$$\frac{V_0}{I_0} = R\frac{\lambda}{l}\left[1 - \frac{R}{R\cosh(l/\lambda) + R_L\sinh(l/\lambda)}\right] \underset{R_L \to +\infty}{\approx} R\frac{\lambda}{l}. \tag{66}$$

The second resistance is more instructive and is associated with the integrated global power balance

$$R'_e = \frac{\int_0^l V(z)\mathcal{I}dz}{\left(\int_0^l \mathcal{I}dz\right)^2}. \tag{67}$$

Indeed, similar to what was discussed for the localized source, the resistance R'_e determines the power balance of the wave or beam driven rotation process for a broad power deposition profile. Using Eq. (65), this resistance rewrites

$$R'_e = R\frac{\lambda}{l}\left[1 - \frac{\lambda}{l}\frac{R\sinh(l/\lambda)}{R\cosh(l/\lambda) + R_L\sinh(l/\lambda)}\right]. \tag{68}$$

Interestingly, we find that

$$R'_e \underset{R_L \to +\infty}{\approx} R\frac{\lambda}{l}, \tag{69}$$

so that the same result is obtained for distributed and localized drives under optimal condition $R_L \to +\infty$. In other words, the power requirement is rather insensitive to the current deposition profile along field lines $0 \leq x \leq l$ when $R_L \to +\infty$ or $l < \lambda$.

B. Voltage shaping

In addition to the power requirement, the model developed here can also be used to study the voltage shaping issue. Indeed, while a careful shaping of the radial power deposition profile can be used to control the radial structure of the electric field, its axial structure is determined by the plasma properties λ, and strategies to control this axial distribution are to be identified. An issue here is that while the assumption $\eta_{\|} = \eta_{\text{Spitzer}}$ is confirmed by experiments in fully ionized plasmas, there exists no large experimental data basis for $\eta_{\perp}$ in fully ionized, magnetized, (supersonic) rotating plasmas. As a result, we cannot accurately calculate the attenuation length λ and the resistance R_e in a fully ionized plasma column of length l. We can, however, as we will do now, identify trends.

Consider first the limit $\lambda > l$. In this limit, the plasma column is not highly dissipative and the power needed to sustain a large radial electric field is small if R_L is large. The large voltage drop is, however, to be handled at the left and right edge of the column with concentric circular end plates, and the issue of the management of high voltage between conductors must then to be solved. Consider now the opposite limit $\lambda < l$. In this limit, the plasma column is rather dissipative and the power needed to sustain a large radial electric field will be large. On the other hand, the insulation of the endplates terminating the field lines will not be a problem. The former situation, that is limited dissipation $\lambda > l$, is the one we will focus on in the remaining of this section.

Consider a plasma column of length l as illustrated in Fig. 8. The wave driven current generator $I_0 = \mathcal{P}_{RF} k_{\perp}/a\omega B$ is assumed to be localized around $z = 0(w)$, and the transverse conductivity $\eta_{\perp}$ is assumed to become very large near $z = \pm l$. This end zone (e) in Fig. 8 can be considered as a short circuit such that $R_L = 0$. With these two boundary conditions, $V(z = l) = 0$ and $I(z = 0) = I_0$, and focusing on the region $z > 0$, the solutions, Eqs. (50) and (51), give

$$I(z) = I_0 \cosh\frac{l-z}{\lambda}\left(\cosh\frac{l}{\lambda}\right)^{-1}, \tag{70}$$

$$V(z) = RI_0 \sinh\frac{l-z}{\lambda}\left(\cosh\frac{l}{\lambda}\right)^{-1}. \tag{71}$$

Symmetrical solutions are expected for $z < 0$, as illustrated in Fig. 8. Note also that we should take $2I_0$ as the wave driven current flows on both the left and right sides of the central region (w).

Although the important problem of how to implement the condition $R_L = 0$ at $z = \pm l$ is left for a future study, we briefly discuss here

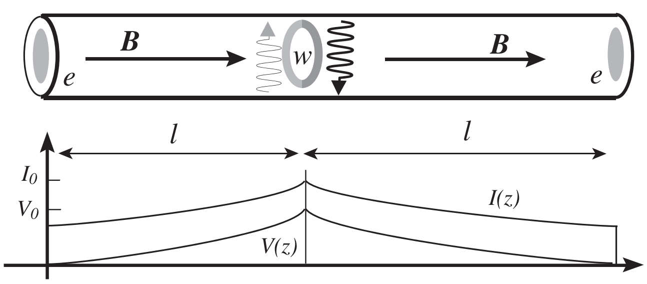

FIG. 8. A magnetized plasma column with two ergodized zone (e) and a central wave/beam driven zone (w).

local ergodization of the magnetic field lines. The required magnetic modulations can be achieved with external coils producing radial and azimuthal components of the magnetic field. The magnetic field lines then display the property of being an Hamiltonian system where the time is replaced by the z coordinate so that the local modulations have several resonances and enter the regime where the Chirikov criterion is fulfilled. The field lines, which are basically the wire along which the free charges flow, will then explore the full radial extent of the zone depicted in gray (e) in Fig. 8, which will provide an almost perfect short circuit between $x = 0$ and $x = a$ in the slab model. Ergodization of magnetic field lines is common in plasma physics and particularly in tokamak plasma where the principle of magnetic island overlapping has been put forward and tested successful with the concept of *ergodic divertor*. Yet, the use of this strategy for the problem at hand raises two problems. First, the short circuit at $z = l$ implies that the power needed to sustain the radial electric field to be very large. From Eq. (71), the power sustaining the generation and confinement of the electric field is

$$I_0 V_0 \approx \frac{RI_0^2 l}{\lambda} = \frac{I_0^2 l}{ab\eta_{\|}}. \tag{72}$$

The plasma slab, thus, behaves as an isotropic conductor with conductivity $\eta_{\|}$. Second, it is not clear that an ergodic zone near the endplates will really protect them from damages as the short circuit will be the source of an intense Joule heating.

Beyond ergodization, alternative strategies to minimize the risk of high voltage damages at the edges of the plasma and to lower the power requirement will have to be established on the specific material and power constraints of each configuration. Equation (57) provides the basis for such analysis. For very large electric fields, and if we let some part of the voltage drop reach the end plates, a preferential combination of electrodes could possibly be used to set up a classical energy recovery system outside the plasma. This part of tolerable voltage will again have to be analyzed with respect to the electrodes properties. Finally, we note that the occurrence of inhomogeneity described in Eq. (49), such as the divergence of magnetic field lines, can in principle be used to shape the axial voltage profile and reduce the electric field on the conducting plates. The examination of these possibilities is left for future studies.

VIII. DISCUSSION AND CONCLUSION

In this first study on wave and beam large electric field generation and control in the core of a magnetized plasmas, we have derived and solved the equation for the axial variation of the voltage drop. We identified R and λ as the control parameters of the problem. We then used these results to address the issue of the power balance and of field shaping in the asymptotic regime $l < \lambda$.

To summarize our findings,

(i) We have identified, proposed, and analyzed two mechanisms for large DC electric field generation inside a magnetized plasma: waves and neutral beams, which are control tools that are already routinely used on modern tokamaks at power levels of the order of tens of Megawatts.[61] The relations Eqs. (21) and (28) provide upper bounds for the electric field theoretically achievable with these wave and beam schemes. These upper bounds are in the GV/m and tens of MV/m ranges for wave and neutral beam drive, respectively.

(ii) We have set up a model of the plasma stationary response to wave and beam power absorption. This model predicts both the electric field penetration from the edge in the classical scheme Fig. 1(a) and the electric field escape from the core central part of a column in the wave or beam driven scheme, Figs. 1(b) and 1(c).
(iii) We have derived the voltage drop equation for an axially inhomogeneous plasma Eq. (49).
(iv) We have identified the three fundamental characteristics of a plasma slab: R, Eq. (40), and λ, Eq. (41), and then calculated the input impedance of the plasma slab R_e, Eq. (57).
(v) We derived in Eq. (61) the minimal power required to sustain a given voltage drop $\mathcal{P}a \sim bl\eta_\perp V_0^2$ and showed that MV/m fields are within the power range of existing wave and beam control devices in large tokamak.

To extend this set of new results, other schemes to localize the voltage drop inside the plasma column, far from the edge, can be explored on the basis of Eq. (49), which is to be completed by appropriate loading or biasing conditions at $s = \int_0^{\pm l} dz/\lambda(z)$.

ACKNOWLEDGMENTS

The authors would like to thank Dr. I. E. Ochs, E. J. Kolmes, T. Rubin, and M. E. Mlodik for constructive discussions. This work was supported by ARPA-E via Grant No. DE-AR001554. J.-M.R. acknowledges Princeton University and the Andlinger Center for Energy + the Environment for the ACEE fellowship, which made this work possible.

AUTHOR DECLARATIONS

Conflict of Interest

The authors have no conflicts to disclose.

Author Contributions

Jean-Marcel Rax: Conceptualization (lead); Formal analysis (lead); Writing – original draft (lead); Writing – review & editing (equal). **Renaud Gueroult:** Conceptualization (supporting); Formal analysis (supporting); Writing – original draft (supporting); Writing – review & editing (equal). **Nathaniel J. Fisch:** Conceptualization (equal); Investigation (supporting); Writing – original draft (supporting); Writing – review & editing (equal).

DATA AVAILABILITY

Data sharing is not applicable to this article as no new data were created or analyzed in this study.

REFERENCES

[1]R. Gueroult, D. T. Hobbs, and N. J. Fisch, J. Hazard. Mater. **297**, 153 (2015).
[2]D. A. Dolgolenko and Y. A. Muromkin, Phys. Usp. **60**, 994 (2017).
[3]A. V. Timofeev, Sov. Phys. Usp. **57**, 990 (2014).
[4]R. Gueroult and N. J. Fisch, Plasma Sources Sci. Technol. **23**, 035002 (2014).
[5]N. A. Vorona, A. V. Gavrikov, A. A. Samokhin, V. P. Smirnov, and Y. S. Khomyakov, Phys. At. Nucl. **78**, 1624 (2015).
[6]V. B. Yuferov, S. V. Shariy, T. I. Tkachova, V. V. Katrechko, A. S. Svichkar, V. O. Ilichova, M. O. Shvets, and E. V. Mufel, Problems At. Sci. Tech. Ser.: Plasma Phys. **107**, 223 (2017).
[7]A. Litvak, S. Agnew, F. Anderegg, B. Cluggish, R. Freeman, J. Gilleland, R. Isler, W. Lee, R. Miller, T. Ohkawa, S. Putvinski, L. Sevier, K. Umstadter, and D. Winslow, in *Proceedings of the 30th EPS Conference on Controlled Fusion and Plasma Physics* (Institute of Physics, 2003), Vol. 27A, p. O-1.6A.
[8]R. Gueroult, J. M. Rax, and N. J. Fisch, J. Clean. Prod. **182**, 1060 (2018).
[9]G. S. Janes, Phys. Rev. Lett. **15**, 135 (1965).
[10]G. S. Janes, R. H. Levy, and H. E. Petschek, Phys. Rev. Lett. **15**, 138 (1965).
[11]G. S. Janes, R. H. Levy, H. A. Bethe, and B. T. Feld, Phys. Rev. **145**, 925 (1966).
[12]J. M. Rax, R. Gueroult, and N. J. Fisch, Phys. Plasmas **24**, 032504 (2017).
[13]I. E. Ochs and N. J. Fisch, Phys. Plasmas **24**, 092513 (2017).
[14]A. B. Hassam, Comments Plasma Phys. Controlled Fusion **18**, 263 (1997).
[15]A. J. Fetterman and N. J. Fisch, Phys. Plasmas **17**, 042112 (2010).
[16]A. J. Fetterman and N. J. Fisch, Phys. Rev. Lett. **101**, 205003 (2008).
[17]C. Teodorescu, W. C. Young, G. W. S. Swan, R. F. Ellis, A. B. Hassam, and C. A. Romero-Talamas, Phys. Rev. Lett. **105**, 085003 (2010).
[18]A. A. Bekhtenev, V. I. Volosov, V. E. Pal'chikov, M. S. Pekker, and Y. N. Yudin, Nucl. Fusion **20**, 579 (1980).
[19]L. Brillouin, Phys. Rev. **67**, 260 (1945).
[20]B. Lehnert, Phys. Scr. **2**, 106 (1970).
[21]B. Lehnert, Phys. Scr. **7**, 102 (1973).
[22]B. Lehnert, Phys. Scr. **9**, 189 (1974).
[23]J. M. Wilcox, Rev. Mod. Phys. **31**, 1045 (1959).
[24]B. Lehnert, Nucl. Fusion **11**, 485 (1971).
[25]J. M. Rax, E. J. Kolmes, I. E. Ochs, N. J. Fisch, and R. Gueroult, Phys. Plasmas **26**, 012303 (2019).
[26]E. J. Kolmes, I. E. Ochs, M. E. Mlodik, J.-M. Rax, R. Gueroult, and N. J. Fisch, Phys. Plasmas **26**, 082309 (2019).
[27]M. Krishnan, M. Geva, and J. L. Hirshfield, Phys. Rev. Lett. **46**, 36 (1981).
[28]T. Ohkawa and R. L. Miller, Phys. Plasmas **9**, 5116 (2002).
[29]S. Shinohara and S. Horii, Jpn. J. Appl. Phys. **46**, 4276 (2007).
[30]R. Gueroult, J.-M. Rax, and N. J. Fisch, Phys. Plasmas **21**, 020701 (2014).
[31]R. Gueroult, E. S. Evans, S. J. Zweben, N. J. Fisch, and F. Levinton, Plasma Sources Sci. Technol. **25**, 035024 (2016).
[32]S. J. Zweben, R. Gueroult, and N. J. Fisch, Phys. Plasmas **25**, 090901 (2018).
[33]R. Gueroult, S. J. Zweben, N. J. Fisch, and J.-M. Rax, Phys. Plasmas **26**, 043511 (2019).
[34]A. J. Fetterman and N. J. Fisch, Plasma Sources Sci. Technol. **18**, 045003 (2009).
[35]A. J. Fetterman and N. J. Fisch, Phys. Plasmas **18**, 094503 (2011).
[36]G. Liziakin, A. Gavrikov, and V. Smirnov, Plasma Sources Sci. Technol. **29**, 015008 (2020).
[37]G. Liziakin, A. Oiler, A. Gavrikov, N. Antonov, and V. Smirnov, J. Plasma Phys. **87**, 905870414 (2021).
[38]G. D. Liziakin, N. N. Antonov, N. A. Vorona, A. V. Gavrikov, S. A. Kislenko, S. D. Kuzmichev, A. D. Melnikov, A. P. Oiler, V. P. Smirnov, R. A. Timirkhanov, and R. A. Usmanov, Plasma Phys. Rep. **48**, 1251 (2022).
[39]K. Flanagan, J. Milhone, J. Egedal, D. Endrizzi, J. Olson, E. Peterson, R. Sassella, and C. Forest, Phys. Rev. Lett. **125**, 135001 (2020).
[40]V. Désangles, G. Bousselin, A. Poyé, and N. Plihon, J. Plasma Phys. **87**, 905870308 (2021).
[41]H. Wiedemann, *Particle Accelerator Physics* (Springer International Publishing, 2015).
[42]J.-M. Rax and N. J. Fisch, Phys. Fluids B **5**, 2578 (1993).
[43]J. M. Rax and N. J. Fisch, Phys. Fluids B **4**, 1323 (1992).
[44]N. J. Fisch and J.-M. Rax, Phys. Rev. Lett. **69**, 612 (1992).
[45]N. Fisch and M. Herrmann, Nucl. Fusion **34**, 1541 (1994).
[46]N. Fisch and M. Herrmann, Nucl. Fusion **35**, 1753 (1995).
[47]M. C. Herrmann and N. J. Fisch, Phys. Rev. Lett. **79**, 1495 (1997).
[48]I. E. Ochs and N. J. Fisch, Phys. Rev. Lett. **127**, 025003 (2021).
[49]I. E. Ochs and N. J. Fisch, Phys. Plasmas **29**, 062106 (2022).
[50]I. E. Ochs and N. J. Fisch, Phys. Plasmas **28**, 102506 (2021).
[51]J. M. Rax, J. Robiche, R. Gueroult, and C. Ehrlacher, Phys. Plasmas **25**, 072503 (2018).
[52]S. V. Putvinskii, Sov. J. Plasma Phys. **7**, 547 (1981).
[53]R. C. Davidson, *Physics of Nonneutral Plasmas* (Imperial College Press, 2001).
[54]F. F. Chen, Phys. Fluids **9**, 965 (1966).

[55] M. J. Hole, R. S. Dallaqua, S. W. Simpson, and E. Del Bosco, Phys. Rev. E **65**, 046409 (2002).
[56] R. Gueroult, J. M. Rax, and N. J. Fisch, Phys. Plasmas **24**, 082102 (2017).
[57] P. Helander and D. J. Sigmar, *Collisional Transport in Magnetized Plasmas* (Cambridge University Press, 2005).
[58] J. M. Rax, *Physique des Plasmas* (Dunod, 2005), p. 425.
[59] R. Gueroult, J.-M. Rax, and N. J. Fisch, Phys. Plasmas **26**, 122106 (2019).
[60] M. J. Poulos, Phys. Plasmas **26**, 022104 (2019).
[61] J. M. Rax, *Physique des Tokamaks* (Editions de l'Ecole Polytechnique, 2011).
[62] B. Trotabas and R. Gueroult, Plasma Sources Sci. Technol. **31**, 025001 (2022).
[63] V. Rozhansky, in *Reviews of Plasma Physics*, Vol. 24, edited by V. D. Shafranov (Springer-Verlag, Berlin Heidelberg, 2008).